Layered BiOCl/$H^+TiNbO_5^-$ heterojunctions for boosting visible-light-driven photocatalytic RhB degradation

Chao Liu[a,1,*], Xin Gao[b,1], Caijun Zhangai[b], Ting Cheng[b], Yan Wang[b], Beibei Zhang[b], Pengyu Dong[c], Xiaowei Chen[a], Xinguo Xi[b,*], Zhigang Zou[d]

[a] School of Materials Science and Engineering, Yancheng Institute of Technology, Yancheng, 224051, P. R. China

[b] School of Chemistry & Chemical Engineering, Yancheng Institute of Technology, Yancheng, 224051, P. R. China.

[c] Key Laboratory for Advanced Technology in Environmental Protection of Jiangsu Province, Yancheng Institute of Technology, Yancheng 224051, China.

[d] Eco-Materials and Renewable Energy Research Centre (ERERC), School of Physics, Nanjing University, Nanjing 210093, P. R. China

*Corresponding authors.

Tel: (+86)-515-8829-8251 (C. Liu); (+86)-515-8829-8186 (X. Xi)

Email addresses: cliu@ycit.edu.cn (C. Liu); xxg@ycit.cn (X. Xi)

[1] Chao Liu and Xin Gao contributed equally to this work.

Characterization

The crystal phase of the obtained samples were confirmed by the powder X-ray diffractometer (XRD, Philip) with Cu Kα irradiation (λ= 1.5418 Å). The morphological information was collected by field-emission scanning electron microscopy (FESEM, JEOL JEM-6300F, Au-coated treatment) and transmission electron microscopy (TEM, JEOL JEM-200CX, acceleration voltage of 200 kV). The samples were deposited onto carbon-coated copper grids for TEM measurement. A JEOL JEM-200CX microscope can be also performed in the scanning transmission mode (STEM) to achieve STEM images using a high angle annular dark field detector (HAADF). UV–vis diffuse reflectance spectroscopy (Shimadzu, UV-3600) was employed to determine optical properties. X-ray photoelectron spectroscopic (XPS) analysis were performed on an X-ray photoelectron spectrometer (Thermo Scientific, Escalab 250 Xi) equipped with a hemispherical electron analyzer (pass energy of 20 eV) and an Al Kα X-ray (hm = 1486.6 eV). Photoluminescence (PL) spectra were recorded on a 48000 DSCF luminescence spectrometer at room temperature by using a continuous-wave 325 nm He-Cd. Raman spectra was obtained by a RENISHAW Raman Microscope from 100 to 3100 cm^{-1}. The N_2 sorption measurements are examined by the Coulter SA 3100 Surface Area and Pore Size Analyzer at 77K.

Photodegradation experiments

Photocatalytic performances of as-prepared samples were observed by photodegradation of rhodamine B (RhB) aqueous solution as the target pollutants. The initial concentration of rhodamine B (RhB) aqueous were 10 $mg \cdot L^{-1}$. Besides, the light source was a 250 W Xenon lamp with a filter (λ > 420 nm). 100 mg of the photocatalyst was dispersed in 100 mL target pollutant aqueous in a glass reactor with a circulating water cooling system. Before the photocatalytic reaction, the suspension was stirring in the darkness lasting 60 min to reach adsorption-desorption equilibrium. After the light on, 4 mL of suspension was drawn out and centrifuged to obtain the supernatant at intervals of 15 min. The concentration of RhB solution and TC aqueous supernatant was explored by the absorption peak at 553 nm and 357 nm respectively with a UV–vis spectrophotometer (Shimadzu UV-2250).

Recycle experiment of photodegradation

To investigate photostability of BTN-3 sample, RhB photodegradation experiment was conducted for four repeated cycles with the detailed processes as follows. For the first cycling experiment, the operation process was the same as that of the above-mentioned photodegradation experiment. After the first cycling reaction, the photocatalyst was fully washed with distilled water and then directly used in the next cycling experiment. The second, third and fourth cycling experiments were conducted using the same operation process as the first cycling experiment. However, the unavoidable weight loss of the catalyst was visible during the recycle experiments.

Photoelectrochemical measurement

The photocurrent and electrochemical impedance spectroscopy (EIS) were investigated by a CHI660D electrochemical workstation with a standard three-electrode frame including a working electrode, a Pt wire as the counter electrode, and Ag/AgCl as a reference electrode. In the photocurrent measurement, the as-fabricated samples (30 mg) and magnesium nitrate (2 mg) were disperised in 20 mL of isopropanol by agitation and ultrasonication for 60 min. Subsequently, the suspension electroplated onto 1 × 1 cm^2 ITO glass which served as the working electrode. The light source was offered by a 300 W Xenon lamp without the filter glasse, the electrolyte was 0.5 $mol \cdot L^{-1}$ Na_2SO_4 solution. The test bias voltage of the photocurrent was set to 0.4 V.

Active species trapping experiment

To explore the generated active species in the photocatalytic degradation process of RhB solution (10 mg/L), different radical scavengers such as ammonium oxalate (AO, 1 mM), tert-butyl alcohol (*t*-BuOH, 5 mM) or p-benzoquinone (BQ, 1 mM) were added to the RhB aqueous solution for capturing active species of hole, $^{\bullet}OH$ and $^{\bullet}O_2^-$, respectively.

Main active species were identified to explore possible photocatalytic mechanism. Electron spin resonance (ESR) signals of the radicals capture by 5, 5-dimethyl pyridine N-oxide (DMPO) were detected by a Bruker model ESR JES-FA200 spectrometer.

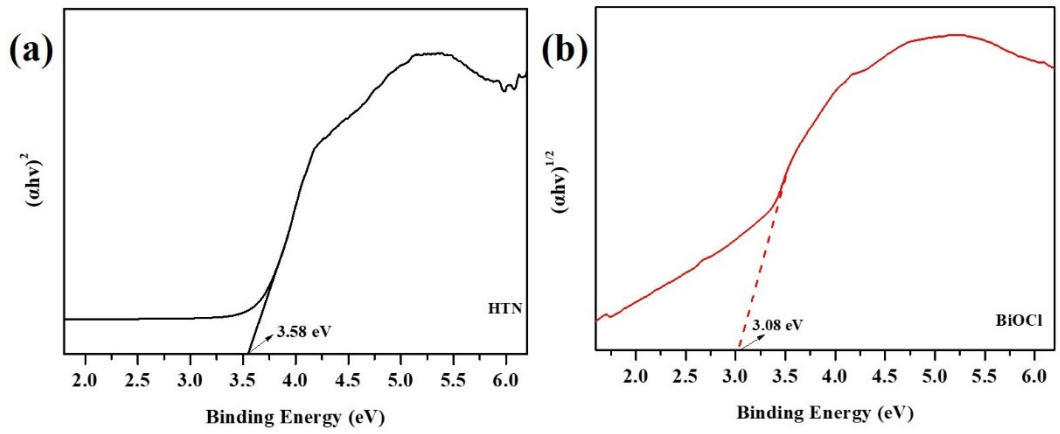

Fig. S1. DRS plots of (a) HTN and (b) BiOCl.

The semiconductor of HTN has a direct transition, while the BiOCl has an indirect transition. Thus, the n values are 2 and 1/2 for the respective HTN and BiOCl [1, 2]. Based on Kubelka-Munk formula, the bandgaps of HTN and BiOCl are calculated to be 3.58 and 3.08 eV, respectively.

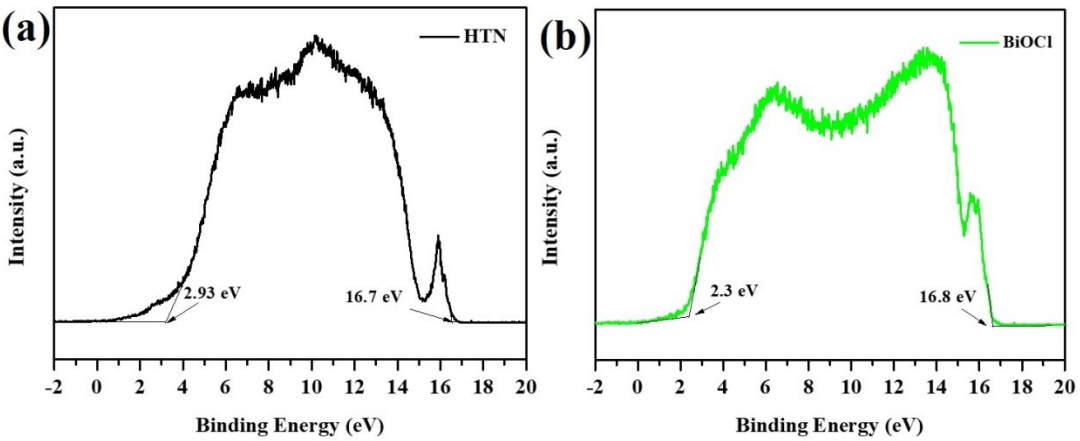

Fig. S2. UPS spectra of (a) HTN and (b) BiOCl nanoplates.

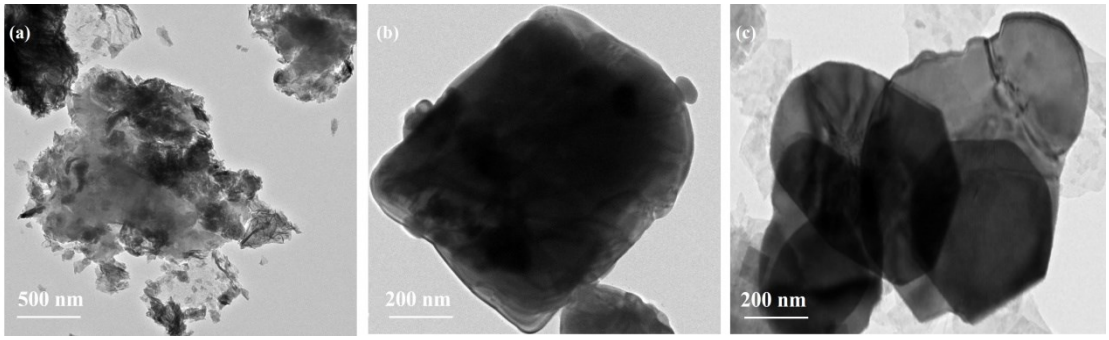

Fig. S3. TEM images of (a) HTN, (b) BiOCl and (c) BTN-3.

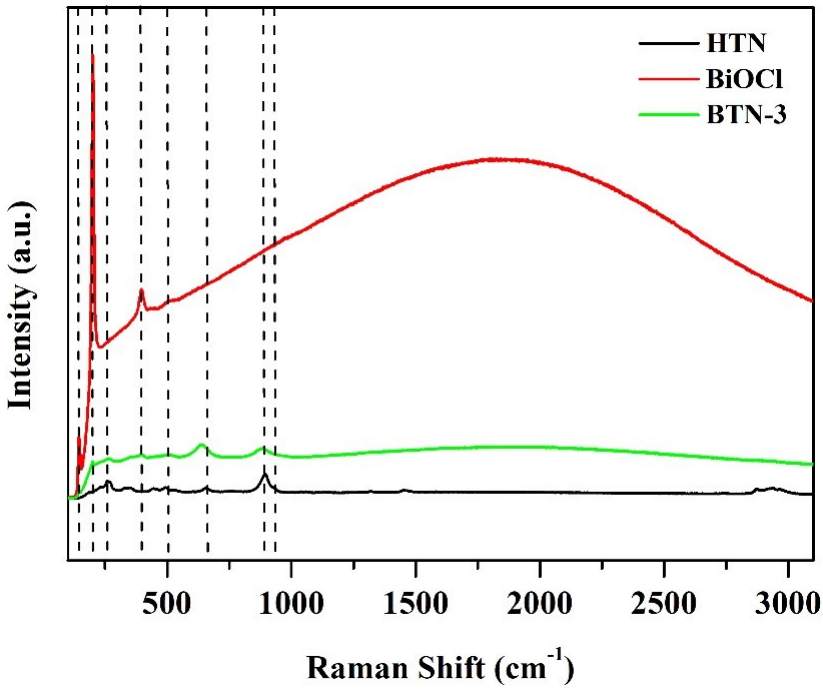

Fig. S4. Raman spectra of HTN, BiOCl and BTN-3.

The structural formulation of the specimens was detected by Raman spectra (Fig. S4). Pure BiOCl shows three characteristic peaks at 141, 204 and 399 cm^{-1}, attributing to overlapping of Bi-Cl stretching (A_{1g}), internal E_g stretching mode (internal Bi-Cl), as well as E_g and B_{1g} bands produced by the motion of oxygen atoms, respectively [3]. Four Raman peaks of HTN sample at 508, 657, 868 and 892 cm^{-1} are ascribed to Ti–O–Ti stretching vibration in edge-shared TiO_6, Nb–O–Nb stretching vibration in edge-shared NbO_6, stretching vibration mode of terminal Ti=O bonds, and the stretching vibration of terminal Nb=O bonds, respectively. The crystalline structure and curvature greatly affected the scattering behavior and peak intensity of Raman spectra [4]. Thus, Raman spectrum of BTN-3 is similar to that of HTN with an obvious position shift, confirming the presence of the strong interaction between HTN and BiOCl in layered BiOCl/HTN heterojunction.

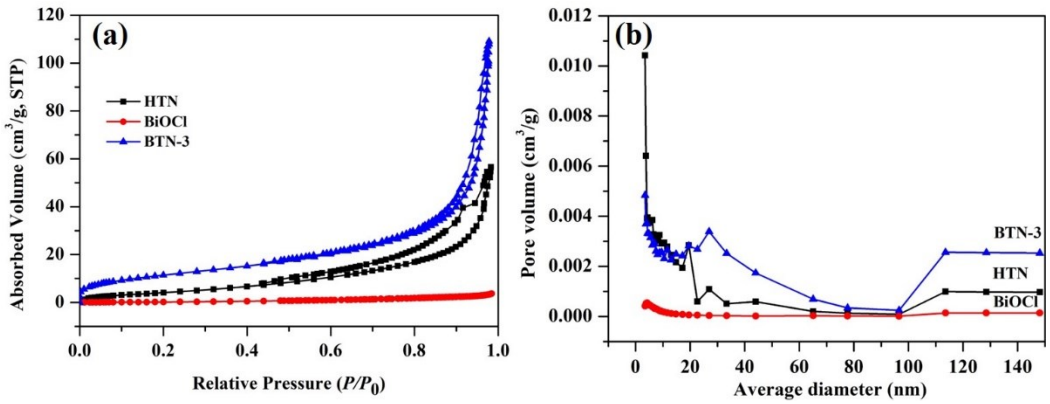

Fig. S5 (a) N_2 adsorption–desorption isotherms, and (b) the pore size distribution curves (adsorption) of HTN, BiOCl and BTN-3.

The specific surface area and the pore structure of as-prepared samples are determined by the nitrogen adsorption/desorption isotherms and pore size distribution curves (Fig. S5). The pure BiOCl shows the type-Ⅰ adsorption isotherm, indicating the nonporous structure. However, the samples of HTN and BTN-3 exhibit type-Ⅱ adsorption isotherm curves, implying the formation of the mesoporous in these two samples. These formed mesoporous are attributed to the accumulated nanosheets. The BTN-3 sample has a highly specific surface area (42.7 $m^2\ g^{-1}$) related to pure BiOCl (0.9 $m^2\ g^{-1}$) and HTN (15.9 $m^2\ g^{-1}$). The increased specific surface area in BTN-3 sample can offer more active sites for photodegradation. In addition, the BTN-3 sample has the pore size distribution at ~27 nm due to the formed slit-like pores, which probably originates from the stacked nanoplates between HTN and BiOCl. The increased specific surface area and porous structure of BTN-3 can offer more active sites, which is beneficial to facilitating photocatalytic activity.

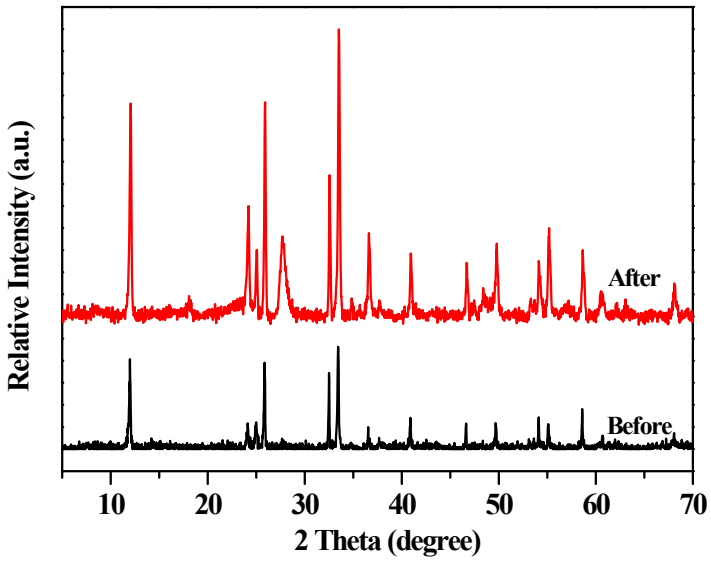

Fig. S6. XRD patterns of the BTN-3 sample before and after photodegradation.

Reference:

[1] Zhai, Z.; Huang, Y. C.; Xu, L.; Yang, X. Y.; Hu, C. H.; Zhang, L. H.; Fan, Y. N.; Hou, W. H.,Thermostable nitrogen-doped $HTiNbO_5$ nanosheets with a high visible-light photocatalytic activity, *Nano Res*. **2011**, *4*, 635–647.

[2] Jiang, S. H.; Zhou, K. Q.; Shi, Y. Q.; Lo, S. M.; Xu, H. Y.; Hu, Y.; Gui, Z., In situ synthesis of hierarchical flower-like Bi_2S_3/BiOCl composite with enhanced visible light photocatalytic activity. *Appl. Surf. Sci*. **2014**, *290*, 313–319.

[3] Seddigi Z, Gondal M, Umair B., Facile synthesis of light harvesting semiconductor bismuth oxychloride nano photo-catalysts for efficient removal of hazardous organic pollutants. *PLOS ONE* **2017,** 12, 0172218.

[4] Wei Y, Guo X, Li B., Exfoliation-co-flocculation fabrication of novel porous $HTiNbO_5$/reduced graphene oxide nanocomposites and the photocatalytic performance. *Micropor Mesopor Mat*. **2019,** 287, 144-151.